Available online at www.sciencedirect.com
ScienceDirect
Journal of Computational Physics 224 (2007) 712–728
JOURNAL OF COMPUTATIONAL PHYSICS
www.elsevier.com/locate/jcp

An improved front tracking method for the Euler equations

J.A.S. Witteveen *, B. Koren, P.G. Bakker

Faculty of Aerospace Engineering, Delft University of Technology, P.O. Box 5058, 2600 GB Delft, The Netherlands

Received 16 March 2006; received in revised form 15 October 2006; accepted 17 October 2006
Available online 28 November 2006

Abstract

An improved front tracking method for hyperbolic conservation laws is presented. The improved method accurately resolves discontinuities as well as continuous phenomena. The method is based on an improved front interaction model for a physically more accurate modeling of the Euler equations, as compared to standard front tracking methods. The resulting algorithm is also more efficient than existing front tracking methods. The improved front tracking method is applied to the Euler equations for one-dimensional unsteady flow and two-dimensional steady supersonic flow. The results are compared to results of a standard front tracking method and a finite volume method.

PACS: 35L65; 35L67; 65M12; 76L05; 76N15

Keywords: Front tracking; Euler equations; Gas dynamics; Hyperbolic conservation laws

1. Introduction

Many problems in fluid dynamics are governed by hyperbolic conservation laws. Their discontinuous solutions can be hard to resolve with standard fixed grid methods. To obtain a more accurate solution in these cases, a fixed grid method can be combined with a front tracking method, in which discontinuities are treated as additional degrees of freedom. Front tracking was initially proposed by Richtmyer and Morton [25] and further developed in the context of aerodynamics by Moretti [24]. It has been applied in a one-dimensional code by for example Swartz and Wendroff [31]. In two-dimensions, front tracking including wave labeling techniques has been investigated by Glimm, Grove, Chern, Holmes and coworkers [2,5,8–11,13,17]. These applications of front tracking have resulted in successful simulations of instabilities [2,13,17] and bifurcations [10] in gas dynamics [5]. It has resulted in increased understanding of hyperbolic systems [8,9] and wave interactions [11]. The extension of front tracking to three dimensions has been demonstrated in [12].

Other types of front tracking methods do not need a fixed background grid for resolving the continuous flow phenomena [27]. These front tracking methods solve for both the continuous and the discontinuous

* Corresponding author. Tel.: +31 15 27 82046; fax: +31 15 27 87077.
E-mail addresses: j.a.s.witteveen@tudelft.nl (J.A.S. Witteveen), b.koren@tudelft.nl (B. Koren), p.g.bakker@tudelft.nl (P.G. Bakker).
URL: http//www.aero.lr.tudelft.nl/~jeroen (J.A.S. Witteveen).

0021-9991/$ - see front matter
doi:10.1016/j.jcp.2006.10.020

phenomena. In that case, the continuous phenomena are represented by a piecewise constant approximation with a series of small discontinuities. In this paper, the latter class of front tracking methods is considered. This version of front tracking can be used as both an analytical and a numerical tool to study hyperbolic conservation laws. As an analytical tool front tracking has been used to analyze scalar equations and systems of hyperbolic conservation laws in one and more spatial dimensions [1,3,4,15,28]. Convergence toward the weak solution has been proven for strictly hyperbolic systems with sufficiently small total variation of the initial data, by Risebro [28], and Bressan and LeFloch [3]. Stability and uniqueness have been demonstrated in [3,4]. In [15] it has been proven that dimensional splitting for scalar conservation laws in multiple spatial dimensions converges to a unique solution. The fact that infinitely many fronts can build up in finite time is discussed in [1,3,28].

Here the front tracking method is considered as a numerical tool to solve problems in fluid dynamics. Front tracking has been used to numerically treat scalar equations and systems of hyperbolic conservations laws [14,20,21,23,26,27]. The front tracking method has for example been applied to one-dimensional problems in gas dynamics and polymer flooding, by Risebro, Tveito and Langseth [20,21,26,27]. Implementation issues have been addressed in [21] and a comparison with Godunov-type methods is given in [20]. In [14], the shallow water equations are treated in combination with operator splitting. A second-order front tracking method for scalar conservations law in one dimension has been developed by Lucier [23]. Front tracking in one-dimension is mainly used as test for multi-dimensional algorithms. In higher dimensions front tracking has been used as a tool in dimensional splitting. In [16,22], the front tracking method is applied to multi-dimensional problems in combination grid adaption, for the scalar case and for systems of conservation laws, respectively.

The basis of a standard front tracking algorithm is the piecewise constant approximation of the solution of local Riemann problems. The position of the discontinuities in this approximation is described by the fronts. In nonlinear initial-boundary value problems these fronts can intersect, which results in front interactions. The flow conditions at the intersection point resemble the initial conditions of a local Riemann problem. The front interaction is solved by computing the solution of the local Riemann problem. The piecewise constant approximation of the solution of the Riemann problem results in new fronts and so on.

The front tracking method is a natural way to solve hyperbolic conservation laws like the Euler equations. However, the standard front tracking method applied to Euler flows [16,27] allows some non-physical behavior, for example: (i) the method is unable to resolve isentropic compressions as truly isentropic phenomena, since a compression in the local Riemann problems is always represented by a non-isentropic shock wave; (ii) after every wave interaction a rarefaction wave is in principle represented by a centered expansion fan like in a standard Riemann problem, and (iii) the difference between left and right running characteristics which can cross each other and characteristics of the same family which cannot cross each other is not modeled explicitly. These shortcomings can be improved by introducing an improved modeling of the physics of front interactions.

An improved front tracking method is introduced based on a theoretical front interaction model that is more general than the standard Riemann problem. The improved front interaction model uses wave front types, which describe the physical phenomena the fronts represent. These wave front types are used in the front interaction model to determine the physically correct interaction pattern. This improved model is based on an analysis of all possible interactions. The improved front tracking method results in a more accurate and a computationally more efficient simulation than existing front tracking methods. In this paper, these properties are demonstrated in one-dimensional unsteady and two-dimensional steady simulations as a test for the implementation in higher dimensions.

The paper is organized as follows: In Section 2, front tracking applied to the Euler equations is briefly reviewed. The improved front tracking method is introduced in Section 3. Numerical results for the Euler equations for one-dimensional unsteady test problems and two-dimensional supersonic wing section flows are presented in Section 4. Finally, in Section 5 the conclusions are summarized.

2. Front tracking applied to the Euler equations

In this section, the basic concepts of front tracking applied to the Euler equations for one-dimensional unsteady flow are briefly reviewed before introducing the improved front interaction method.

The system of hyperbolic conservation laws which describes one-dimensional unsteady Euler flow is given by

$$\frac{\partial U}{\partial t}+\frac{\partial F(U)}{\partial x}=0,\quad U=\begin{pmatrix}\rho\\ \rho u\\ \rho E\end{pmatrix},\quad F=\begin{pmatrix}\rho u\\ p+\rho u^2\\ \rho u H\end{pmatrix}, \tag{1}$$

and initial condition $U(x,0)=U_0(x)$, with ρ the density, u the velocity, p the pressure, $H=E+\frac{p}{\rho}$ the enthalpy, E the internal energy, which for a perfect gas reads $E=\frac{1}{\gamma-1}\frac{p}{\rho}+\frac{1}{2}u^2$, with γ the ratio of specific heats ($\gamma=\frac{c_p}{c_v}$), and with $U_0(x)$ the initial condition, see for example [6,29].

The first step in solving the Cauchy problem for the Euler equations (1) with a front tracking method is to approximate the initial conditions by a piecewise constant function. This introduces a first-order error in the L_1-norm. At the discontinuities in this approximation, the initial conditions resemble those of a local Riemann problem [32]. In Fig. 1, a Riemann problem is show with the initial condition of two constant states U_{left} and U_{right}. The solution of the Riemann problem for the Euler equations, generally consists of three waves: a left and right running shock or rarefaction wave and a contact discontinuity in between, see for example [6,29]. Four different constant states can be identified in the solution of the Riemann problem, where the two middle states only differ in their densities.

The pressure and the velocity in the middle states, p_{middle} and u_{middle}, can be solved for in the p,u-state space by determining the intersection point of the two curves representing the left and the right running waves. In general, this solution has to be determined iteratively. A non-isentropic compression by means of a shock wave is represented by the Hugoniot curve. A rarefaction wave is represented by the Poisson curve. The Poisson curve also describes an isentropic compression.

The solutions of the local Riemann problems in the piecewise constant approximation of the initial condition are approximated by a piecewise constant functions. This approximation is exact for a shock wave and a contact discontinuity. A continuous rarefaction fan is approximated by a piecewise constant function with a series of discontinuities. This results in a first-order accurate approximation in the L_1-norm [27]. The position of the discontinuities in space-time is described by the fronts. In intersection points of fronts the solution resembles the initial condition of a local Riemann problem. The solution of the local Riemann problem is again approximated by a piecewise constant function and so on. The one-dimensional front tracking algorithm as reviewed in this section is usually extended to higher dimensions as a tool in dimensional splitting, see for example [16].

The accuracy of the solution depends on the number of discontinuities that are used to approximate a rarefaction fan. Increasing this number results in a first-order error convergence. In theory, the number of fronts in the solution of a Cauchy problem can be unbounded [1,3,28]. This problem is avoided numerically

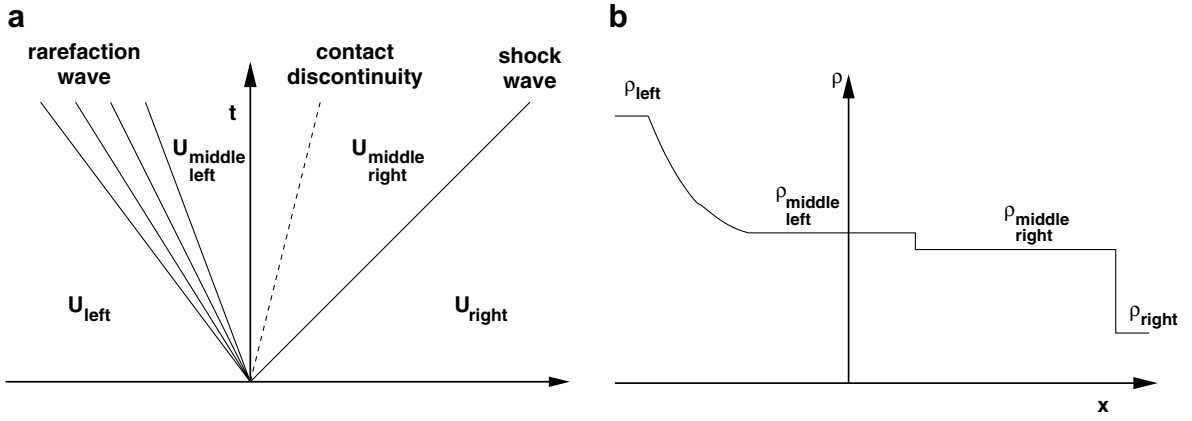

Fig. 1. A typical solution of the Riemann problem for the Euler equations for one-dimensional unsteady flow.

by ignoring small discontinuities. This results in a computationally efficient method without affecting the error convergence significantly.

3. The improved front tracking method

For using the front tracking method as a numerical tool, it is important that the flow physics is modeled correctly. In a front tracking algorithm the flow physics is modeled by the front interaction model. In the standard front tracking algorithm [16,27] the front interaction modeling is fully determined by solving standard Riemann problems. However, just solving standard Riemann problems at the intersection points allows some non-physical behavior.

In this section, the improved front interaction model is introduced to obtain a more accurate simulation of the physical behavior. The front interaction model is improved by taking into account that the intersecting fronts represent specific physical phenomena. These wave phenomena interact differently with each other in terms of the wave pattern that is generated at the intersection point. This wave pattern can differ from the wave pattern generated by a standard Riemann problem. For example, if two characteristics of different families intersect, the same waves are present after the intersection. Solving a standard Riemann problem in that case results in the creation of shock waves or centered rarefaction fans.

Using theoretical gas dynamics [6,29,34] the wave pattern associated with every front interaction can be determined. The actual front velocities and the flow conditions are computed by solving a local Riemann problem. Riemann problems are now solved in a non-standard way, since the solution depends on the wave pattern that is prescribed by the front interaction model. Important numerical properties of the front tracking method, like the error convergence and conservation properties, depend on the discretization of rarefaction fans.

First, in Section 3.1 the wave types are reviewed, which are used to describe the physical phenomena the fronts represent. In Section 3.2 the front interaction model based on the wave types is described. The non-standard Riemann solver which depends on the created wave pattern is discussed in Section 3.3. In Section 3.4, a discretization of rarefaction waves with equally spaced fronts is considered.

3.1. The wave types

The basic waves in Euler flows are a shock wave, a rarefaction or compression fan, and a contact discontinuity [6,29]. In Fig. 2a the wave types in the discretization of a Riemann problem are shown. In the piecewise constant approximation of the solution of the Riemann problem, shock waves are discretized by a single front. Such a front is assigned the wave type of shock wave (sw), of which the velocity u_{sw} is given by the Rankine–Hugoniot relation $u_{sw}\Delta U = \Delta F$, where ΔU and ΔF are the jumps over the shock wave of the state and the flux vector, respectively.

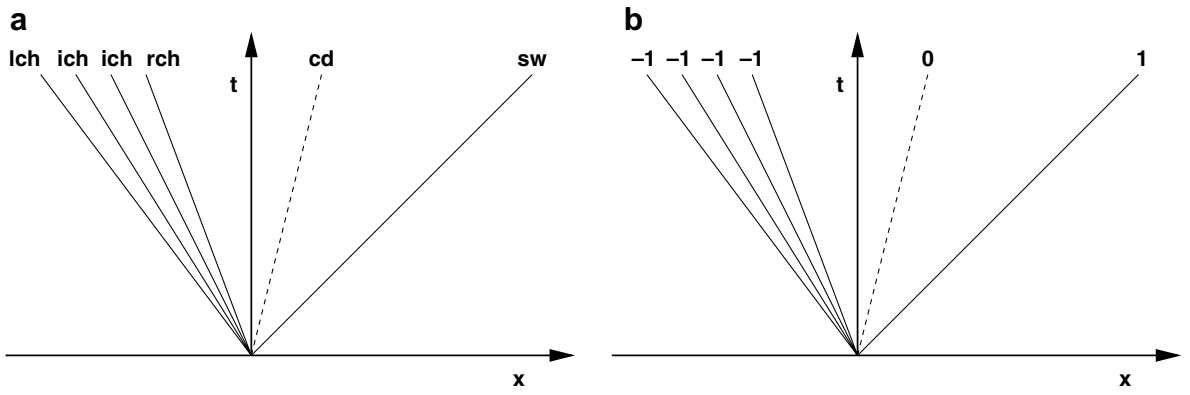

Fig. 2. The wave types and wave family types in the discretization of a Riemann problem.

A rarefaction wave consists of a fan of characteristics. The fronts in the piecewise constant approximation of a rarefaction fan therefore represent the wave type of a characteristic. To discretize the spatial dimension of a rarefaction fan accurately, three different wave types are used for representing characteristics. The left end of a rarefaction wave is discretized by a front with the leftmost characteristic (lch) wave type with the characteristic velocity $u_{\mathrm{lch}} = (u \pm c)_{\mathrm{L}}$, where the minus sign holds for a left running characteristic and the subscript L denotes the state immediately at the left of the rarefaction wave as a whole. Similarly, the right end of a rarefaction fan is discretized by a front with the rightmost characteristic (rch) wave type with velocity $u_{\mathrm{rch}} = (u \pm c)_{\mathrm{R}}$, where the subscript R denotes the state immediately at the right of the rarefaction wave.

The spatial dimension of a rarefaction fan can be represented by using one leftmost characteristic (lch) and one rightmost characteristic (rch). For a more accurate discretization of the solution inside a rarefaction wave, more than two fronts are used. These other fronts have the interior characteristic (ich) wave type with velocity $u_{\mathrm{ich}} = \frac{1}{2}((u \pm c)_{\mathrm{l}} + (u \pm c)_{\mathrm{r}})$, where the subscripts l and r denote the flow conditions immediately at the left and the right of the interior front, respectively. The characteristic wave types are also used in the discretization of isentropic compression fans, see Fig. 3a.

A contact discontinuity is discretized by a single front with the contact discontinuity (cd) wave type. The velocity of the contact discontinuity wave type $u_{\mathrm{cd}} = u_{\mathrm{L,R}}$ is equal to the flow velocity immediately left and right of the contact discontinuity. In the solution of the Riemann problem this velocity corresponds to the velocity in the middle state of the solution $u_{\mathrm{cd}} = u_{\mathrm{middle}}$. Continuous variations of entropy, like for example in the shock wave–rarefaction wave interaction of Fig. 3b, are discretized by a series of fronts representing contact waves (cw). Three contact wave types are used: the leftmost front (lcw), the rightmost front (rcw) and an interior front (icw) of a continuous change of entropy. The velocity of the waves lcw, rcw and icw is equal to the flow velocity immediately left and right of the contact wave.

Also a family type is assigned to the fronts. Front interactions are influenced by the relative velocity of the intersecting waves with respect to the fluid. The sign of this relative velocity is known as the family of the wave. For example, two intersecting characteristics of different families can cross each other, but intersecting characteristics of the same family form a shock wave. All fronts are assigned one of the following three families of waves: left running waves (−1), right running waves (1) and waves which have no relative velocity with respect to the surrounding fluid (0). Shock waves and rarefaction waves can have wave family type (−1) or (1) depending on whether they are created as left or right waves in a local Riemann problem. Contact waves have wave family type (0). In Fig. 2b the wave family types in the discretization of a Riemann problem are shown.

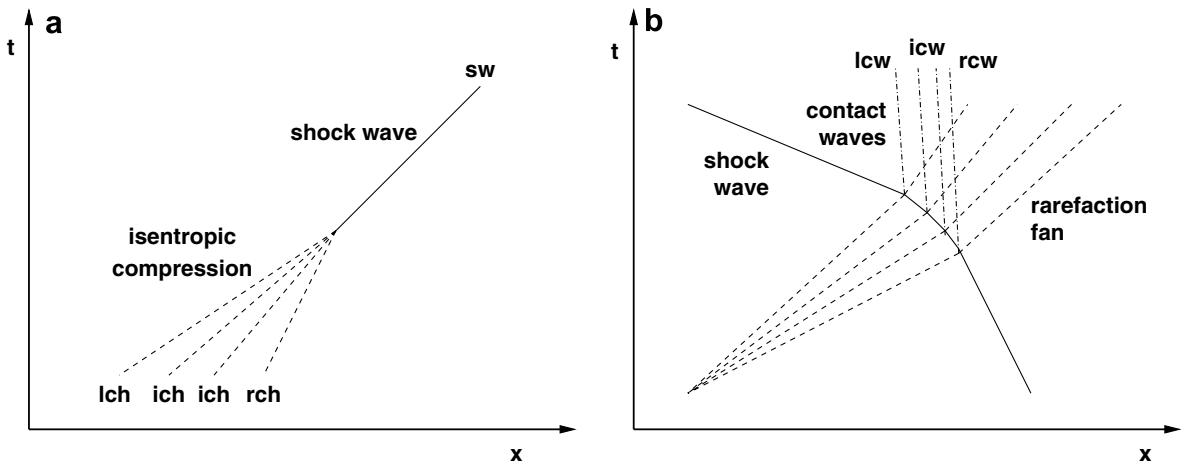

Fig. 3. Examples of the discretization of two continuous flow phenomena.

3.2. The front interaction model

The front interaction model determines the solution of the front interaction in terms of the wave types of the created wave pattern. The wave pattern is a function of the wave types and the families of the intersecting waves. The 12 different combinations of wave types and family types result in 144 different wave intersections. However, only 70 different wave intersections are physically possible. For example, two fronts with relative velocity family (0) cannot intersect.

Every created wave pattern consists potentially of a left, right and middle wave. The improved front interaction model prescribes the wave types of these waves. The left and the right wave types can be shock wave (sw), characteristic (lch, rch and ich) or the origin of a new rarefaction fan consisting of a series of characteristics. The middle wave is always a contact discontinuity or a contact wave type (cd, lcw, rcw and icw). The left and right wave family are left (-1) and right (1) running, respectively. The middle wave does not have a relative velocity with respect to the flow which corresponds to family (0). For all possible wave intersections the created wave types can be derived from theoretical gas dynamics. In Appendix A the improved front interaction model is given in tabulated form.

The front velocities and the flow conditions after the front interaction are computed by solving the local Riemann problem at the intersection point. This Riemann solver has to take into account the effect of the wave types prescribed by the front interaction model. After solving the local Riemann problem, the front interaction is fully resolved. The fronts with wave types and wave families prescribed by the front interaction model and computed front velocities are added to the space-time solution. If a centered rarefaction fan is created, it is discretized by a series of characterics fronts. To avoid the build up of an infinite number of fronts, weak fronts in the created wave pattern are neglected.

As an example consider the intersection of two left running characteristics of wave type ich, see Fig. 4. In that case the front interaction model, see Appendix A, prescribes the creation of a shock wave as left wave $(\mathrm{sw}, -1)$, a rightmost characteristic as right wave $(\mathrm{rch}, 1)$ and a rightmost contact wave as middle wave $(\mathrm{rcw}, 0)$. The solution of the local Riemann problem determines the velocities of the three new fronts and the flow states between the left, middle and right front.

3.3. The Riemann solver

The front interaction model determines whether the waves are isentropic or possibly non-isentropic before solving the Riemann problem. This information has to be taken into account by the Riemann solver by representing non-isentropic waves by a Hugoniot curve and isentropic waves by a Poisson curve. The solution of the Riemann problem in the p,u-state space is then the intersection point of the curves representing the left and

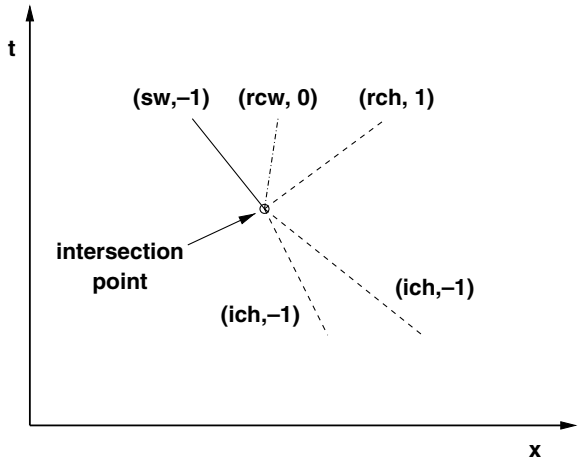

Fig. 4. Example of a wave interaction of two left running (-1) characteristics of wave type ich.

the right wave. Four different Riemann solvers are implemented for the four different combinations of isentropic and non-isentropic waves. This enables resolving isentropic compression waves as truly isentropic phenomena.

For solving the isentropic Riemann problem the analytical solution is used. For the other Riemann problems an efficient iterative algorithm is used based on an iteration using the isentropic solution and similar to the one described by Emanuel [7]. In this iteration the flow velocity and the pressure of the middle state u_{middle} and p_{middle} are approximated by the intersection point of the Poisson curves through the initial left and right states U_{left} and U_{right}, respectively. If the left or right wave are a shock wave in the wave pattern prescribed by the front interaction model and the wave is a compression wave, then the left or right pressure of the middle state is updated to lie on the corresponding Hugoniot curve. In the next iteration the flow velocity and the pressure of the middle state u_{middle} and p_{middle} are updated to the intersection point of the Poisson curves through the left and right states U_{left} and U_{right} found in the previous iteration, etc. This iteration is repeated until the absolute value of the difference of the pressures of the middle states is smaller than a user defined stop criterion. Cavity formation has not been considered in the Riemann solver for the current applications.

The computational time of the front tracking method is dominated by solving the Riemann problems. The improved front interaction model reduces the average number of iterations per Riemann problem compared to a standard front tracking method. In the improved front tracking method compression waves are represented by isentropic compression waves when physically appropriate. In a standard front tracking method every compression wave is represented by a shock wave. The interaction of isentropic waves is more easy to compute than when a non-isentropic wave is involved. This results in a smaller number of total iterations for solving the Riemann problems in the improved front tracking method.

3.4. The discretization of rarefaction waves

The discretization of rarefaction fans is important for the error convergence rate and the conservation properties of the front tracking method. Here a discretization of rarefaction waves with equally spaced fronts is considered. The number of fronts that discretize a rarefaction fan depends on the strength of the rarefaction wave defined by

$$\Delta_{\text{w}} = \frac{1}{3}\left(\frac{|u_{\text{L}} - u_{\text{R}}|}{\frac{1}{2}(|u_{\text{L}}| + |u_{\text{R}}|)} + \frac{|p_{\text{L}} - p_{\text{R}}|}{\frac{1}{2}(p_{\text{L}} + p_{\text{R}})} + \frac{|\rho_{\text{L}} - \rho_{\text{R}}|}{\frac{1}{2}(\rho_{\text{L}} + \rho_{\text{R}})}\right). \tag{2}$$

The wave strength is also used for neglecting fronts weaker than a user-defined value ε_{w}. Dividing the wave strength (2) of the rarefaction wave by a user-defined constant δ_{rw} gives the number of fronts N_{f} that discretize the rarefaction fan:

$$N_{\text{f}} = \max\left\{2, \left\lceil \frac{\Delta_{\text{w}}}{\delta_{\text{rw}}} \right\rceil\right\}. \tag{3}$$

Let $\{f_1, f_2, \ldots, f_{N_{\text{f}}}\}$ be the sequence of fronts that discretize the rarefaction fan from left to right. The fronts $\{f_i\}_{i=1}^{N_{\text{f}}}$ separate domains with uniform states $\{U_1, U_2, \ldots, U_{N_{\text{f}}-1}\}$, such that the domain with state U_i is enclosed at the left by front f_i and at the right by f_{i+1}, for $i = 1, 2, \ldots, N_{\text{f}} - 1$. Then the wave types of fronts f_1 and $f_{N_{\text{f}}}$ are lch and rch, respectively. The other fronts $\{f_2, \ldots, f_{N_{\text{f}}-1}\}$ have wave type ich. The wave velocities of fronts f_1 and $f_{N_{\text{f}}}$ are $u_{\text{lch}} = (u \pm c)_{\text{L}}$ and $u_{\text{rch}} = (u \pm c)_{\text{R}}$, respectively. The velocities of the ich waves vary linearly from the velocity of the leftmost front to the velocity of the rightmost front:

$$u_{\text{ich},i} = u_{\text{lch}} + (u_{\text{rch}} - u_{\text{lch}})\frac{i-1}{N_{\text{f}} - 1}, \quad i = 2, 3, \ldots, N_{\text{f}} - 1. \tag{4}$$

For rarefaction fans with linear velocity distributions, this results in equally spaced fronts inside the rarefaction fan. The flow velocity u_{f_i} and the speed of sound c_{f_i} on the ith front can be determined by isentropic relations. The piecewise constant flow conditions in between the fronts are determined by three relations. The first relation is the relation for the velocity of the ich waves as defined in Section 3.1:

$$u_{\mathrm{ich},i} = \frac{1}{2}\left((u \pm c)_{i-1} + (u \pm c)_i\right), \quad i = 2, 3, \ldots, N_\mathrm{f} - 1, \tag{5}$$

where $u_{\mathrm{ich},i}$ is given by (4). Since a rarefaction fan is an isentropic phenomenon, the second relation is the isentropic relation

$$\frac{p}{\rho^\gamma} = \text{constant}. \tag{6}$$

Satisfying this relation is important for preventing the creation of spurious numerical contact waves. For the third relation the conservation of mass is used. Integrating the conservation of mass in state space between the fronts f_i and f_{i+1} results in

$$\rho_i = \frac{\int_{u_{f_i}}^{u_{f_{i+1}}} \rho \, \mathrm{d}u}{u_{f_{i+1}} - u_{f_i}}, \quad i = 1, 2, \ldots, N_\mathrm{f} - 1. \tag{7}$$

The same relations are used for discretizing isentropic compression fans.

4. Numerical results

In this section, the improved front tracking method is applied to five test problems. Three one-dimensional unsteady test problems (Sod's Riemann problem, an isentropic compression, a standard blast-wave problem) and two supersonic wing section flows are considered. These problems are of interest for one-dimensional unsteady and two-dimensional supersonic problems and as tests for implementation in a fully multi-dimensional algorithm. For these test problems the error convergence, the computational work and the conservation error are studied. The results are compared to results of a standard front tracking method and a finite volume method.

4.1. Sod's Riemann problem

The solution of the Riemann problem is an important part of the front tracking algorithm. Therefore, the first test problem is Sod's Riemann problem [30,32]. This test problem is used to verify the improved front tracking method with respect to error convergence and conservation error. The initial conditions for Sod's Riemann problem are

$$\begin{aligned} u_\mathrm{l} &= 0, \quad u_\mathrm{r} = 0, \\ p_\mathrm{l} &= 1, \quad p_\mathrm{r} = 0.1, \\ \rho_\mathrm{l} &= 1, \quad \rho_\mathrm{r} = 0.125. \end{aligned}$$

The solution at $t = 1$ is computed. In Fig. 5, the solution of the improved front tracking method in space-time and the density at $t = 1$ are given. In Fig. 5a the rarefaction fan is discretized by 8 fronts. In Fig. 5b the solution for the density ρ for 8 and 1024 fronts is shown. In Fig. 6 the convergence of the global discretization error and conservation errors at $t = 1$ are compared to the results of a standard front tracking method. The following L_1-error measure is used for the global discretization error

$$\frac{\|u(x,t) - u_\mathrm{ref}(x,t)\|_1}{\|u_\mathrm{ref}(x,t)\|_1} + \frac{\|p(x,t) - p_\mathrm{ref}(x,t)\|_1}{\|p(x,t)_\mathrm{ref}\|_1} + \frac{\|\rho(x,t) - \rho_\mathrm{ref}(x,t)\|_1}{\|\rho_\mathrm{ref}(x,t)\|_1}. \tag{8}$$

The conservation error is given by

$$\left| \int_{D(t)} U(x,t)\,\mathrm{d}x - \int_{D(0)} U(x,0)\,\mathrm{d}x \right| \tag{9}$$

plus contributions of the domain boundaries, where $D(t)$ is the spatial domain. The results of the improved and the standard front tracking method for this test problem are identical, since no front intersections occur. The error convergence as a function of the number of fronts discretizing the expansion fan N_f is first-order as

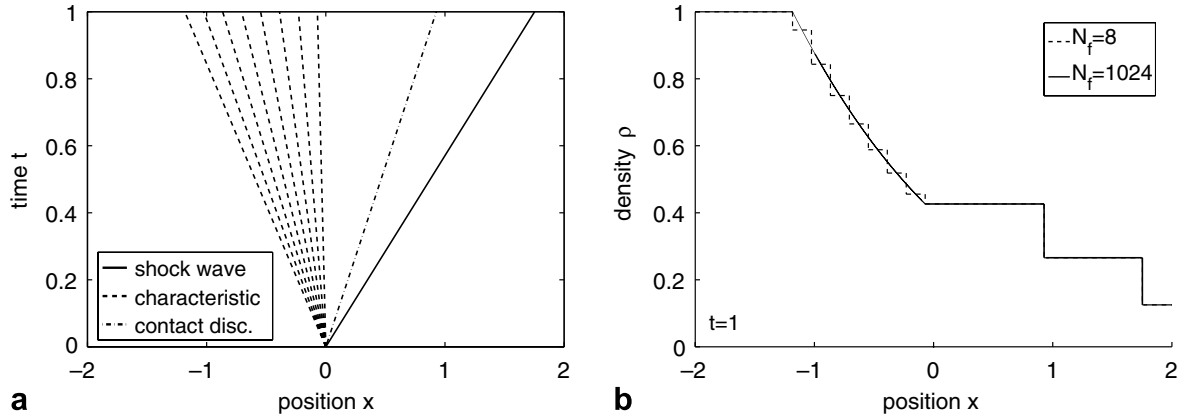

Fig. 5. Solution of the improved front tracking method for Sod's Riemann problem.

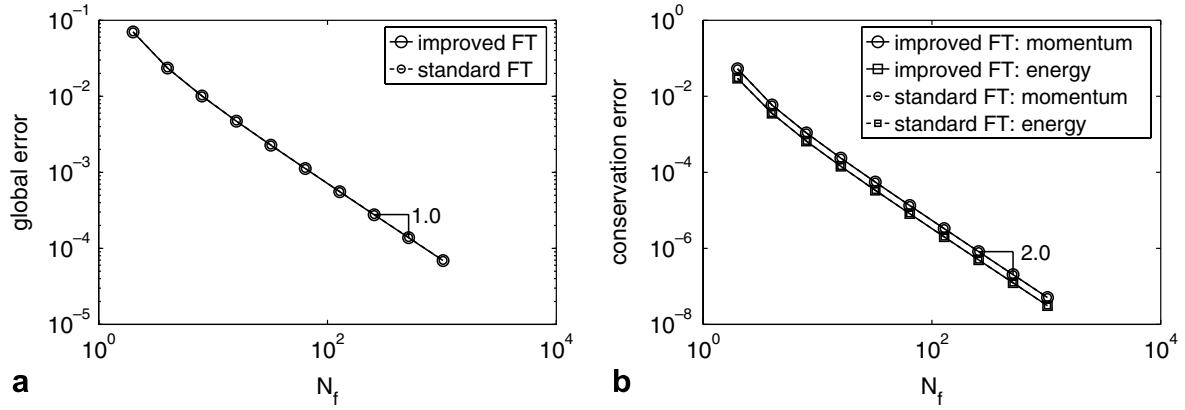

Fig. 6. L_1 norm of the global discretization error and conservation errors of the improved and standard front tracking (FT) method as a function of the number of fronts N_f discretizing the rarefaction fan, for Sod's Riemann problem.

expected [27]. The conservation of mass is satisfied up to machine precision, since the conservation of mass (7) is used to determine the density inside the rarefaction fan. The conservation of mass is only restricted by the accuracy of the Riemann solver. The conservation of momentum and energy reach second-order convergence similar as reported in [31].

4.2. An isentropic compression

The next test problem is a one-dimensional unsteady piston problem with an isentropic compression, see Fig. 7. This test problem is used to demonstrate that the improved front tracking method resolves isentropic compressions more accurately than a standard front tracking method. At $t = 0$, the piston at the left of the semi-infinite fluid domain starts to move to the right with a constant acceleration of $\frac{1}{2}$. The piston creates an isentropic compression fan in which a shock wave is formed after finite time $t = 1.1$. The shock strength increases in time, which causes a continuous change of entropy behind the shock wave. This entropy layer is discretized by a series of contact waves. The piston path is discretized by using a piecewise linear approximation using N_p points. The number of fronts discretizing the isentropic compression fan is then: $N_f = N_p$.

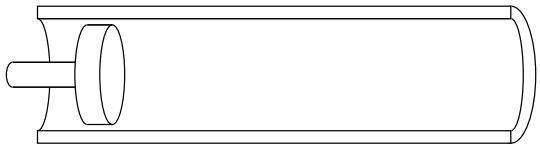

Fig. 7. The piston problem with a piston closing the semi-infinite fluid domain at the left.

In Fig. 8a the solution in space-time is given for $t \in [0; 1.4]$. In Fig. 8b the entropy at $t = 1.4$ is shown for $N_f = 6$ for both the improved and the standard front tracking method. The results are compared to the solution of the improved front tracking method with $N_f = 64$. It can be seen that the improved front tracking method results in an exactly isentropic compression fan independent of the accuracy of the discretization and that the entropy increases only due to the increasing strength of the shock wave. The standard front tracking method results in an entropy error behind the isentropic part of the compression.

The error convergence and the computational work for the improved and standard front tracking method are given in Fig. 9. Both methods are first-order accurate with respect to N_f, see Fig. 9a. The entropy error has an effect on the global discretization error, but it does not affect the convergence rate. Resolving isentropic compressions can have a large effect on the efficiency. For front tracking methods the computational work is dominated by solving the Riemann problems. Therefore, a good measure for the amount of computational work for a front tracking method is the total number of Riemann solver iterations needed. In Fig. 9b the computational work is given as a function of N_f. For this flow problem, the amount of computational work with the improved front tracking method is a factor two lower than with the standard front tracking method. The solution of Riemann problems involving shock waves requires more iterations than an isentropic Riemann problem. Since in a standard front tracking method all compressions are represented by shock waves, a

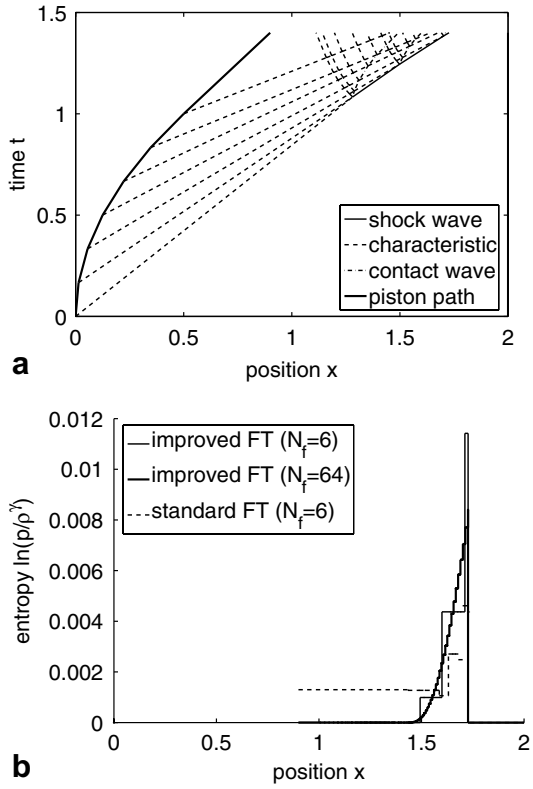

Fig. 8. The improved and standard front tracking (FT) method for a piston problem with an isentropic compression for $t \in [0; 1.4]$.

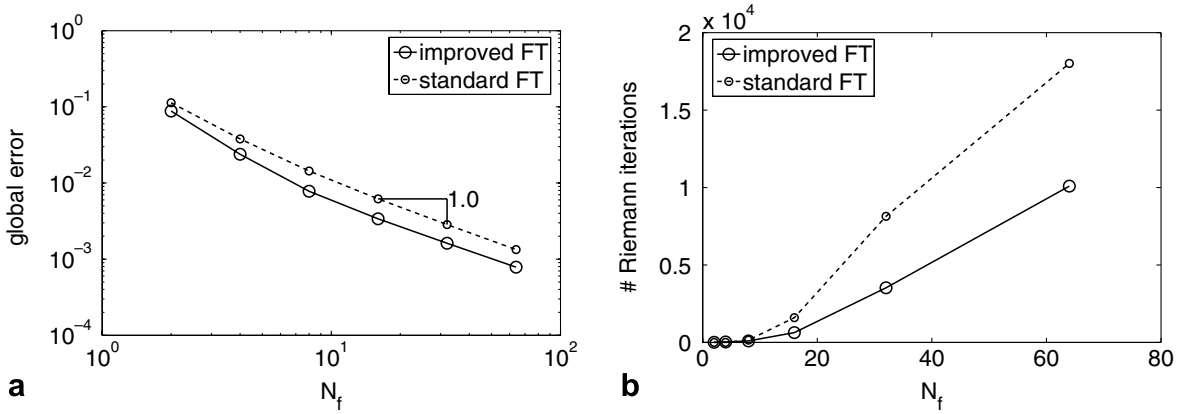

Fig. 9. L_1-norm of the global discretization error and the computational work of the improved and standard front tracking (FT) method for the piston problem with an isentropic compression.

standard front tracking method is computationally more intensive than the improved front tracking method. The conservation error converges again with second-order.

4.3. The blast-wave problem

The blast-wave test problem of Woodward and Colella [33] is a standard test problem for demonstrating the performance of numerical methods with respect to resolving strong shock waves, rarefaction fans and contact discontinuities. The blast-wave test problem is defined in a one-dimensional spatial domain with unit length. The fluid is enclosed by a reflecting wall at both ends. Initially, the fluid is divided into three uniform domains with zero velocity, unit density and pressure:

$$p = \begin{cases} 1000, & 0 < x < 0.1, \\ 0.01, & 0.1 < x < 0.9, \\ 100, & 0.9 < x < 1. \end{cases} \tag{10}$$

From these discontinuities in the initial condition, two shock waves and two contact discontinuities run toward the center of the domain and two centered rarefaction fans run toward the walls at which they reflect, such that all these flow phenomena interact with each other in the interior of the flow domain.

In Fig. 10 the solution of the improved front tracking method for the blast-wave test problem is given for $t \in [0; 0.038]$. In Fig. 10a the solution for the space-time domain for $\delta_{rw} = 0.25$ is shown in terms of the front paths and wave types. In Fig. 10b the density at $t = 0.038$ is given for $\delta_{rw} = 0.05$. By comparing these two figures with results in [33], it can be concluded that the solution is very accurate. The solution shown in Fig. 10b has been obtained by using only 7938 cells in the whole space-time domain. It is remarked that in the reference solution in [33] already 3096 cells are used per time step. This demonstrates the efficiency of the improved front tracking method. The computational time is dominated by solving in total 7616 Riemann problems in the intersection points. For this test problem, the average number of iterations per Riemann problem is only 1.13, due to the large number of isentropic Riemann problems.

In Fig. 11, the error convergence is shown versus δ_{rw} and the amount of computational work. The error convergence of the improved front tracking method is first-order, see Fig. 11a. The results of the standard front tracking method are not shown in the same figure, since the relative wave strength defined by (2) cannot be used for a standard front tracking method. For the standard front tracking method an absolute measure of the wave strength is used. The error convergence as a function of the computational work for both methods is shown in Fig. 11b. The improved front tracking method appears to result in a faster convergence than the standard front tracking method. The reduction in computational work is due to (i) the relatively higher

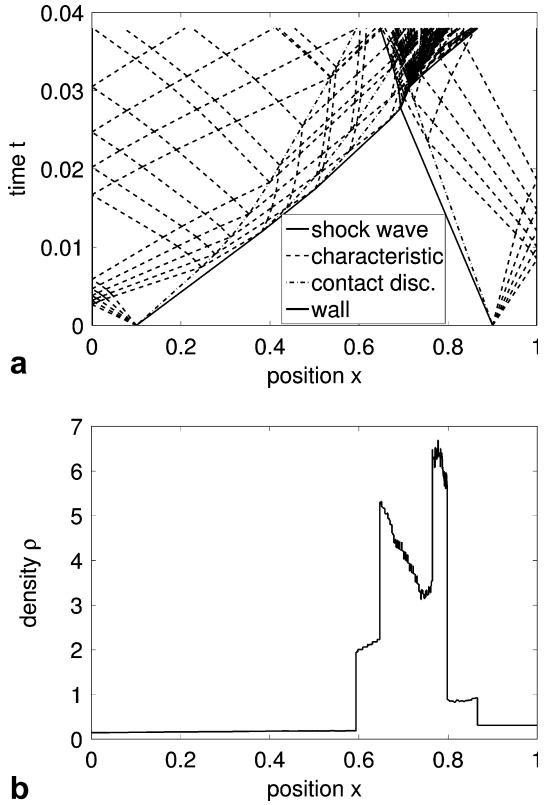

Fig. 10. The improved front tracking method for the blast-wave problem for $t \in [0; 0.038]$.

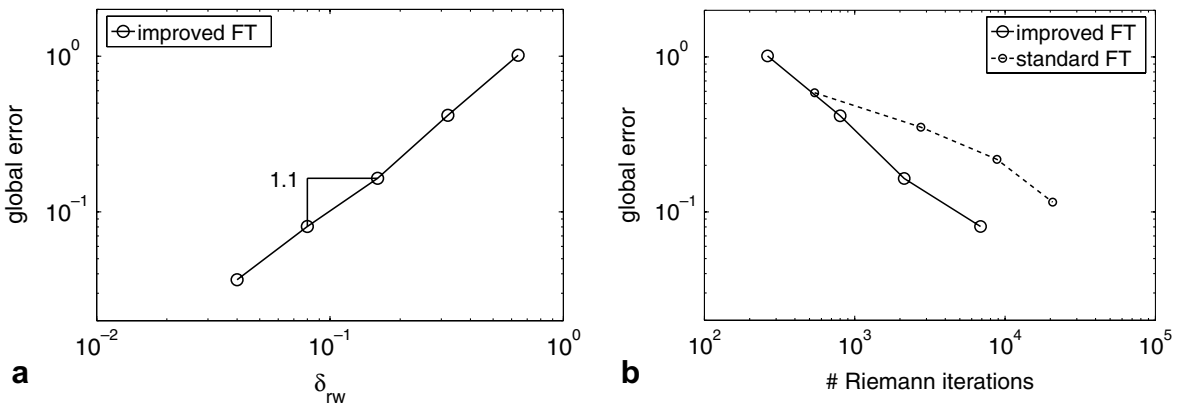

Fig. 11. L_1-norm of the global discretization error of the improved and standard front tracking (FT) method, for the blast-wave problem.

number of isentropic front interactions for the improved front tracking method and (ii) the definition of the relative wave strength.

4.4. Supersonic wing section flow

The front tracking method can also be applied to the steady Euler equations for two-dimensional supersonic flow. In this section, the improved front tracking method is applied to supersonic wing section flows. A diamond shaped wing section and a parabolic wing section are considered.

4.4.1. The Euler equations for two-dimensional supersonic flow

The Euler equations for two-dimensional steady flow are given by

$$\frac{\partial F}{\partial x}+\frac{\partial G}{\partial y}=0,\quad F=\begin{pmatrix}\rho u\\ p+\rho u^2\\ \rho uv\\ \rho uH\end{pmatrix},\quad G=\begin{pmatrix}\rho v\\ \rho uv\\ p+\rho v^2\\ \rho vH\end{pmatrix}, \tag{11}$$

with u and v the velocity components in x- and y-direction, respectively. If the flow is supersonic in the whole flow field, these equations are hyperbolic in the flow direction. The wave types and the front interactions remain the same as for the one-dimensional unsteady case. For applying the improved front tracking method to steady two-dimensional supersonic flow only minor changes in the algorithm have to be made: (i) Riemann solvers for the supersonic two-dimensional steady Riemann problem have to be used and (ii) an extra variable has to be introduced to describe the second component of the velocity vector.

4.4.2. A diamond shaped wing section

The first wing section that is considered is a diamond shaped wing section with a maximum thickness of $y_{\max}=0.1$ at $x=\frac{1}{2}$. The Mach number of the undisturbed flow is $M_\infty=1.5$. The results of the front tracking method are compared to results of a finite volume method [18,19]. The computations with the finite volume method are performed with second-order accuracy by using a limiter scheme on a 96×96-grid. A multigrid method is used to speed up the solution process.

In Fig. 12 the numerical solutions for the pressure field are shown. The result of the improved front tracking method is given in Fig. 12a. In Fig. 12b the solution of the finite volume method is shown. The improved front tracking method results in a clearly more accurate solution. In the improved front tracking method numerical diffusion is absent. In the finite volume method the numerical diffusion results in significant smearing of the shock waves. The spatial grid of the improved front tracking method is significantly coarser than that of the finite volume method due to a reduction of the number of cells with a factor 100.

4.4.3. A parabolic wing section

The second wing section is parabolic with a maximum thickness of $y_{\max}=0.1$ at $x=\frac{1}{2}$. The undisturbed Mach number is again $M_\infty=1.5$. For the numerical treatment the parabolic wing section shape is approximated piecewise linearly. This piecewise linear function is handled by the improved front tracking method as a continuous variation in curvature (except for the leading and trailing edge). In Figs. 13a and 13b the solution of the improved front tracking method and the finite volume method, respectively, are shown. For the

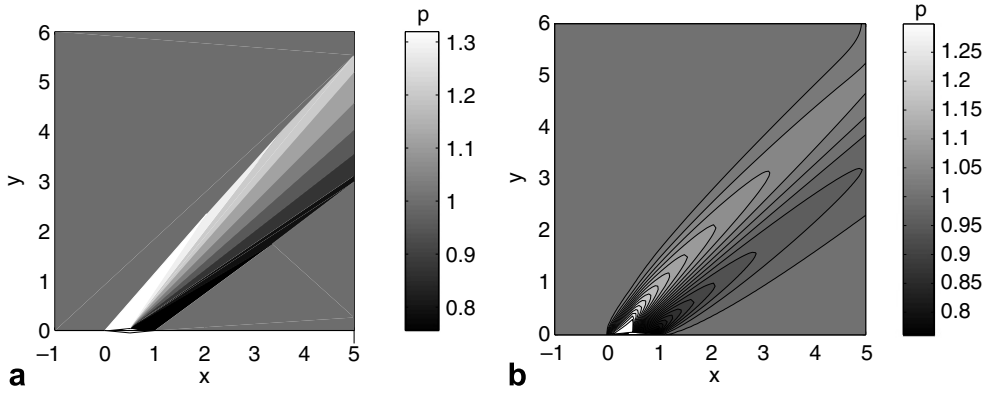

Fig. 12. Pressure distribution of the improved front tracking method compared to that of a finite volume method, for a two-dimensional supersonic flow over a diamond shaped wing section at $M_\infty=1.5$.

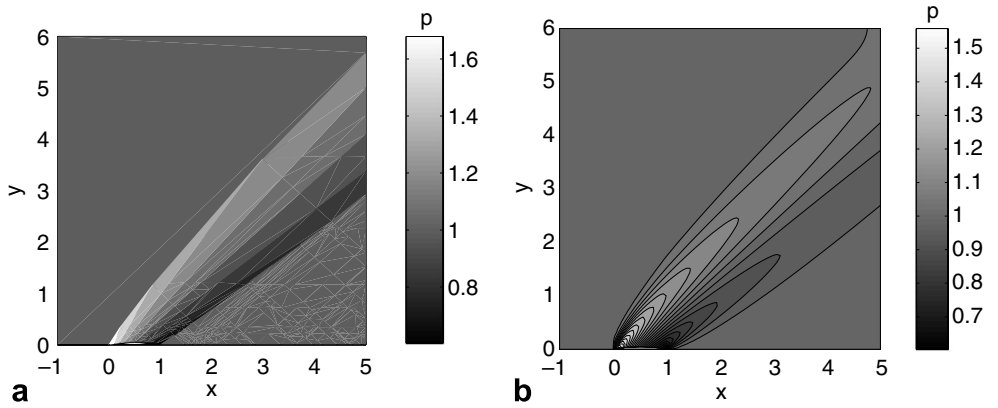

Fig. 13. Pressure distribution of the improved front tracking method compared to that of a finite volume method for a two-dimensional supersonic flow over a parabolic wing section at $M_\infty = 1.5$.

parabolic wing section, the improved front tracking method results in a similar improvement of the accuracy and efficiency compared to the finite volume method.

5. Conclusions

An improved front tracking method has been presented for solving the Euler equations numerically. A front tracking method approximates the solution by a piecewise constant function with a series of discontinuities. The position of these discontinuities is described by the fronts. In the improved front tracking method besides the position and the strength of the discontinuities, also the physical phenomena that the fronts represent, are tracked. This information is used in an improved front interaction model for a better physical modeling of the Euler equations. This results in a more accurate simulation and less computational work than with a standard front tracking method. The improved front tracking method is more efficient due to the decrease of the average number of iterations per Riemann problem and due to the use of a relative measure for the wave strength.

These properties have been demonstrated by applying the improved front tracking method to test problems for the Euler equations. One-dimensional unsteady shock tube problems have been considered, i.e. Sod's Riemann problem, a piston problem and a standard blast-wave problem. The results have been compared to those of a standard front tracking method. The improved front tracking method has also been applied to supersonic wing section flows. The results have been compared to those of a finite volume method there. The error convergence rate of the improved front tracking method is first-order which is standard for front tracking methods. The conservation errors converge with second-order. It is demonstrated for the blast-wave problem that the improved front tracking method is up to a factor 10 times more efficient than a standard front tracking method. Compared to a finite volume method, the improved front tracking method is more accurate, since numerical dissipation is absent. Moreover, the computational grid resulting from the improved front tracking method is significantly coarser. These results motivate a further study into the implementation in a fully multi-dimensional algorithm as a tool in dimensional splitting.

Appendix A. The front interaction model in tabulated form

In this appendix the improved front interaction model is given in tabulated form. The front interaction model prescribes the wave types of the fronts that are created in the local Riemann problem solved at the intersection point of fronts. The prescribed wave types are a function of the wave types and the wave families of the intersecting fronts. Only intersections of two fronts are considered here. In Tables A.1–A.3 the wave types of the created left, middle and right wave are given as a function of the intersecting left and right front, respec-

Table A.1
The improved front interaction model for the created left wave type (family −1)

type	right	sw	sw	lch	lch	rch	rch	ich	ich	cd	lcw	rcw	icw
left	fam.	−1	1	−1	1	−1	1	−1	1	0	0	0	0
sw	−1	sw	×	sw	×	sw	×	sw	×	×	×	×	×
sw	1	sw	rw	lch	lch	rch	rch	ich	ich	rw	lch	rch	ich
lch	−1	sw	×	×	×	sw	×	sw	×	×	×	×	×
lch	1	sw	rch	lch	×	rch	rw	ich	lch	rch	ich	rch	ich
rch	−1	sw	×	×	×	×	×	×	×	×	×	×	×
rch	1	sw	lch	lch	×	rch	×	ich	×	lch	lch	ich	ich
ich	−1	sw	×	×	×	sw	×	sw	×	×	×	×	×
ich	1	sw	ich	lch	×	rch	lch	ich	lch	ich	ich	ich	ich
cd	0	sw	×	lch	×	rch	×	ich	×	×	×	×	×
lcw	0	sw	×	lch	×	rch	×	ich	×	×	×	×	×
rcw	0	sw	×	lch	×	rch	×	ich	×	×	×	×	×
icw	0	sw	×	lch	×	rch	×	ich	×	×	×	×	×

Table A.2
The improved front interaction model for the created middle wave type (family 0)

type	right	sw	sw	lch	lch	rch	rch	ich	ich	cd	lcw	rcw	icw
left	fam.	−1	1	−1	1	−1	1	−1	1	0	0	0	0
sw	−1	cd	×	rcw	×	lcw	×	icw	×	×	×	×	×
sw	1	cd	cd	lcw	lcw	rcw	rcw	icw	icw	cd	lcw	rcw	icw
lch	−1	lcw	×	×	×	cd	×	rcw	×	×	×	×	×
lch	1	lcw	rcw	–	×	–	cd	–	lcw	cd	lcw	rcw	icw
rch	−1	rcw	×	×	×	×	×	×	×	×	×	×	×
rch	1	rcw	lcw	–	×	–	×	–	×	cd	lcw	rcw	icw
ich	−1	icw	×	×	×	rcw	×	rcw	×	×	×	×	×
ich	1	icw	icw	–	×	–	lcw	–	lcw	cd	lcw	rcw	icw
cd	0	cd	×	cd	×	cd	×	cd	×	×	×	×	×
lcw	0	lcw	×	lcw	×	lcw	×	lcw	×	×	×	×	×
rcw	0	rcw	×	rcw	×	rcw	×	rcw	×	×	×	×	×
icw	0	icw	×	icw	×	icw	×	icw	×	×	×	×	×

Table A.3
The improved front interaction model for the created right wave type (family 1)

type	right	sw	sw	lch	lch	rch	rch	ich	ich	cd	lcw	rcw	icw
left	fam.	−1	1	−1	1	−1	1	−1	1	0	0	0	0
sw	−1	rw	×	rch	×	lch	×	ich	×	×	×	×	×
sw	1	sw	sw	sw	sw	sw	sw	sw	sw	sw	sw	sw	sw
lch	−1	lch	×	×	×	rw	×	rch	×	×	×	×	×
lch	1	lch	sw	lch	×	lch	sw	lch	sw	lch	lch	lch	lch
rch	−1	rch	×	×	×	×	×	×	×	×	×	×	×
rch	1	rch	sw	rch	×	rch	×	rch	×	rch	rch	rch	rch
ich	−1	ich	×	×	×	rch	×	rch	×	×	×	×	×
ich	1	ich	sw	ich	×	ich	sw	ich	sw	ich	ich	ich	ich
cd	0	rw	×	rch	×	lch	×	ich	×	×	×	×	×
lcw	0	lch	×	rch	×	lch	×	ich	×	×	×	×	×
rcw	0	rch	×	rch	×	lch	×	ich	×	×	×	×	×
icw	0	ich	×	rch	×	lch	×	ich	×	×	×	×	×

tively. Vertically, the 12 different wave type combinations with relative velocity family of the left intersecting wave are given. Horizontally, the wave type and wave family of the right intersecting wave are given. The wave types are shortened as follows:

sw, shock wave;
lch, leftmost characteristic of a fan of characteristics;
rch, rightmost characteristic of a fan of characteristics;
ich, internal characteristic of a fan of characteristics;
cd, contact discontinuity;
lcw, leftmost contact wave of a continuous change in entropy;
rcw, rightmost contact wave of a continuous change in entropy;
icw, internal contact wave of a continuous change in entropy.

The wave families are denoted as:

−1, left running wave;
1, right running wave;
0, zero relative velocity wave.

See Section 3.1 for a more detailed description of the wave types and the wave families. In Table A.1 the wave types of the created left waves (family −1) are tabulated for every combination of intersecting fronts. The intersections which are impossible are denoted by a ×. The wave type of the left waves cannot be a contact discontinuity wave type. In some cases the created wave can be either a shock wave or a centered rarefaction fan depending on the solution of the Riemann problem. This is denoted by rw.

In Table A.2 the wave types of the created middle waves (family 0) are tabulated for every combination of intersecting fronts. The wave type is always a contact wave or contact discontinuity wave type. If no middle wave is created at the intersection this is denoted by the symbol −. In Table A.3 the wave types of the created right waves (family 1) are tabulated for every combination of intersecting fronts. The wave type of a right wave cannot be a contact discontinuity wave type.

References

[1] P. Baiti, H.K. Jenssen, On the front tracking algorithm, J. Math. Anal. Appl. 217 (1998) 395.
[2] B. Boston, J.W. Grove, R.L. Holmes, Shock induced surface instabilities and non-linear wave interactions, Math. Contemp. 8 (1995) 39.
[3] A. Bressan, P. LeFloch, Uniqueness of weak solution to systems of conservation laws, Arch. Rational Mech. Anal. 140 (1997) 301.
[4] A. Bressan, G. Crasta, B. Piccoli, Well-posedness of the Cauchy problem for $n \times n$ systems of conservation laws, Mem. Am. Math. Soc., Providence, 2000.
[5] I.-L. Chern, J. Glimm, O. McBryan, B. Plohr, S. Yaniv, Front tracking for gas dynamics, J. Comput. Phys. 62 (1986) 83.
[6] A.J. Chorin, J.E. Marsden, A Mathematical Introduction to Fluid Mechanics, Springer-Verlag, New York, 1979.
[7] G. Emanuel, Analytical Fluid Dynamics, CRC Press, Boca Raton, 2001.
[8] J. Glimm, E. Isaacson, D. Marchesin, O. McBryan, Front tracking for hyperbolic systems, Adv. Appl. Math. 2 (1981) 91.
[9] J. Glimm, C. Klingenberg, O. McBryan, B. Plohr, D. Sharp, S. Yaniv, Front tracking and two-dimensional Riemann problems, Adv. Appl. Math. 6 (1985) 259.
[10] J. Glimm, J. Grove, B. Lindquist, O. McBryan, G. Tryggvason, The bifurcation of tracked scalar waves, SIAM J. Sci. Stat. Comput. 9 (1988) 61.
[11] J. Glimm, The interaction of nonlinear hyperbolic waves, Commun. Pur. Appl. Math. 41 (1988) 569.
[12] J. Glimm, J.W. Grove, X.L. Li, K.-M. Shyue, Y. Zeng, Q. Zhang, Three-dimensional front tracking, SIAM J. Sci. Comput. 19 (1998) 703.
[13] J.W. Grove, Applications of front tracking to the simulation of shock refractions and unstable mixing, J. Appl. Numer. Math. 14 (1994) 213.
[14] R. Holdahl, H. Holden, K.-A. Lie, Unconditionally stable splitting methods for the shallow water equations, BIT 39 (1999) 451.
[15] H. Holden, N.H. Risebro, A method of fractional steps for scalar conservation laws without the CFL condition, Math. Comput. 60 (1993) 221.
[16] H. Holden, K.-A. Lie, N.H. Risebro, An unconditionally stable method for the Euler equations, J. Comput. Phys. 150 (1999) 76.
[17] R.L. Holmes, J.W. Grove, D.H. Sharp, Numerical investigation of Richtmyer–Meshkov instability using front tracking, J. Fluid Mech. 301 (1995) 51.
[18] B. Koren, Defect correction and multigrid for an efficient and accurate computation of airfoil flows, J. Comput. Phys. 77 (1988) 183.

[19] B. Koren, Euler flow solutions for transonic shock wave–boundary layer interaction, Int. J. Numer. Meth. Fluids 9 (1989) 59.
[20] J.O. Langseth, N.H. Risebro, A. Tveito, A conservative front tracking scheme for 1D hyperbolic conservation laws, in: A. Donato et al. (Eds.), Nonlinear Hyperbolic Problems: Theoretical, Applied, and Computational Aspects, Notes Numer. Fluid Mech, vol. 43, Vieweg, Braunschweig, 1993, p. 385.
[21] J.O. Langseth, On an implementation of a front tracking method for hyperbolic conservation laws, Adv. Eng. Software 26 (1996) 45.
[22] K.-A. Lie, V. Haugse, K.H. Karlsen, Dimensional splitting with front tracking and adaptive grid refinement, Numer. Meth. Part. D.E. 14 (1998) 627.
[23] B.J. Lucier, A moving mesh numerical method for hyperbolic conservation laws, Math. Comput. 173 (1986) 59.
[24] G. Moretti, Computations of flows with shocks, Ann. Rev. Fluid Mech. 19 (1987) 313.
[25] R. Richtmyer, K. Morton, Difference Methods for Initial Value Problems, Interscience, New York, 1967.
[26] N.H. Risebro, A. Tveito, Front tracking applied to a nonstrictly hyperbolic system of conservation laws, SIAM J. Sci. Statist. Comput. 12 (1991) 1401.
[27] N.H. Risebro, A. Tveito, A front tracking method for conservation laws in one dimension, J. Comput. Phys. 101 (1992) 130.
[28] N.H. Risebro, A front tracking alternative to the random choice method, Proc. Am. Math. Soc. 117 (1993) 1125.
[29] J. Smoller, Shock Waves and Reaction-diffusion Equations, second ed., Springer-Verlag, New York, 1994.
[30] G.A. Sod, A survey of several finite difference methods for systems of nonlinear hyperbolic conservation laws, J. Comput. Phys. 27 (1978) 1.
[31] B.K. Swartz, B. Wendroff, AZTEC: a front tracking code based on Godunov's method, Appl. Numer. Math. 2 (1986) 385.
[32] E.F. Toro, Riemann Solvers and Numerical Methods for Fluid Dynamics, Springer Verlag, Berlin, 1997.
[33] P.R. Woodward, P. Colella, The numerical simulation of two-dimensional flow with strong shocks, J. Comput. Phys. 54 (1984) 115.
[34] R.D. Zucker, O. Biblarz (Eds.), Fundamentals of Gas Dynamics, second ed., Wiley, Hoboken, 2002.